

Comparison of far-ultraviolet emission lines formed in coronal holes and the quiet Sun

K. Stucki¹, S.K. Solanki², U. Schühle², I. Ruedi³, K. Wilhelm², J.O. Stenflo¹, A. Brković¹, and M.C.E. Huber⁴

¹ ETH-Zentrum, Institute of Astronomy, 8092 Zürich, Switzerland

² Max-Planck-Institut für Aeronomie, 37191 Katlenburg-Lindau, Germany

³ PMOD/WRC, 7260 Davos Dorf, Switzerland

⁴ European Space Agency, Space Science Department, ESTEC, P.O. Box 299, 2200 AG Noordwijk, The Netherlands

Received 21 July 2000 / Accepted 21 September 2000

Abstract. We present an analysis of 26 far-ultraviolet emission lines belonging to 19 atoms and ions observed on both sides of the boundary of polar coronal holes as well as other quiet Sun areas along the limb. The observations were made with the SUMER instrument (Solar Ultraviolet Measurements of Emitted Radiation) onboard the Solar and Heliospheric Observatory (SOHO). We compare line intensities, shifts and widths in coronal holes with the corresponding values obtained in the quiet Sun. We find that with increasing formation temperature, spectral lines show on average an increasingly stronger blueshift in coronal holes relative to the quiet Sun at equal heliospheric angle, with the coolest lines in our sample (formation temperature $\approx 10^4$ K) indicating a small relative redshift. With respect to the rest wavelength, however, only lines formed above $5 \cdot 10^5$ K show blueshifts in coronal holes, which is not very different from the quiet Sun. The width of the lines is generally larger (by a few kilometers per second) inside the coronal hole. Intensity measurements clearly show the presence of the coronal hole in Ne VIII lines as well as in Fe XII, and provide evidence for a slightly enhanced emission in polar coronal holes for lines formed below 10^5 K. This last result is, however, less certain than the rest due to relatively poor statistics. Intensity histograms also exhibit distinct differences between coronal hole and quiet-Sun data. For cooler chromospheric lines, such as Ni II, the coronal holes display a greater spread in intensities than the quiet Sun. Transition-region lines, e.g. O IV, do not reveal such differences, while Ne VIII shows characteristics of a coronal line with lower average intensity and lower intensity spread inside holes.

Key words: Sun: corona – Sun: solar wind – Sun: transition region – Sun: UV radiation

1. Introduction

Coronal holes are the source of the fast solar wind and the primary example of coronal heating in regions with a significant

excess of one magnetic polarity (Hollweg 1991; Marsch 1997), but are not yet well understood. Intensity distribution measurements with Skylab revealed the presence of coronal holes at different temperatures (Huber et al. 1974). Nevertheless, before the advent of SOHO, only a limited amount of data was available, often hampered by limited spatial resolution or sampling. The possibility provided by SUMER of observing line profiles at high spatial resolution allows us to determine plasma properties, in particular flows and turbulent velocities in the chromosphere, transition region and lower corona. Distinctive differences in center-to-limb intensity variations of lines between coronal holes and quiet-Sun regions have been reported by Wilhelm et al. (1998a). Recently, blueshifted emission in coronal holes has been reported by Hassler et al. (1999) and Peter (1999) in Ne VIII 770.43 Å, and by Wilhelm et al. (2000) in He I 584.33 Å and Ne VIII 770.43 Å.

Here, we report on a comparison of high spatial and spectral resolution data of coronal-hole and quiet-Sun areas located along the limb. Our investigation is based on data recorded on the solar disk, which differs from many other studies of coronal hole characteristics that place the emphasis on off-limb data (e.g., Wilhelm et al. 1998b; Tu et al. 1998). Also, we concentrate on results obtained from a large number of spectral lines (26) at the expense of large spatial sampling, in contrast to Hassler et al. (1999), Wilhelm et al. (2000), Dammasch et al. (1999), who analyse data with better spatial statistics, but in fewer lines. We also study the differences between intensity distributions in coronal holes and the quiet Sun, and compare the results with those obtained by Huber et al. (1974) using Skylab data.

2. Observations, data reduction and analysis

2.1. Observational data

The observations have been carried out using the SUMER Spectrometer (Solar Ultraviolet Measurements of Emitted Radiation) onboard the Solar and Heliospheric Observatory, SOHO. This instrument allows high-resolution solar observations over a broad wavelength range of approximately 500–1610 Å (extreme ultraviolet). The detectors have opaque KBr photocathode material deposited over the central half of their areas, while

Send offprint requests to: K. Stucki

Correspondence to: kstucki@astro.phys.ethz.ch

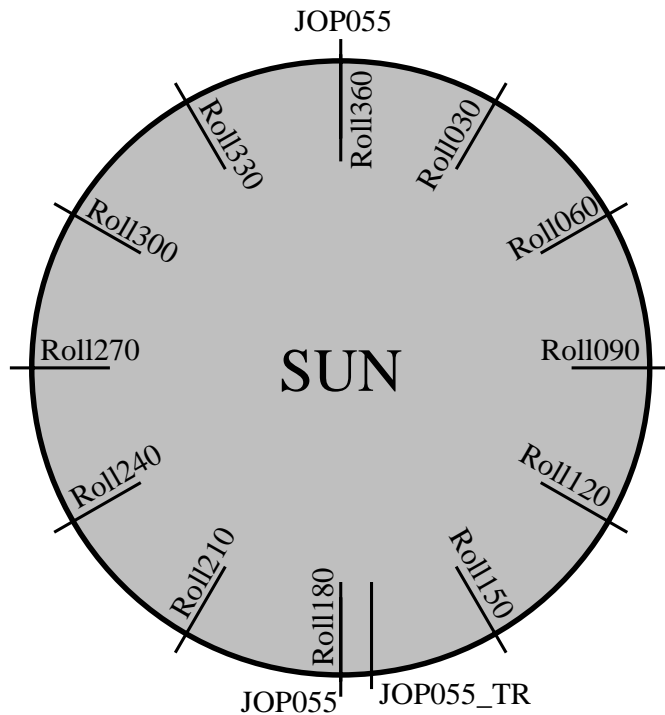


Fig. 1. Position of the different observation sets on the Sun: JOP055, JOP55_TR and Roll data

the two sides consist of bare microchannel plates. A detailed description of the SUMER instrument, its specifications and capabilities is provided by Wilhelm et al. (1995). Our observations were recorded using detector B and a long slit which covers $1'' \times 300''$ of the solar disk.

Three sets of observations were used. The first set (Joint Observing Programme JOP055) was obtained between the 10th and 17th of December 1996. This JOP was run 12 times. Each time, 14 different spectral frames were recorded and read out ($1024 \text{ spectral} \times 360 \text{ spatial pixels}$), each exposed for 300 s with the slit position at the central meridian, where it crossed the boundary of either the northern or the southern coronal hole. As the slit location is very close to the pole, no rotation compensation was necessary. The 14 frames cover a large part of the spectrum between 730 and 1420 \AA , including more than 70 identified and relatively unblended spectral lines.

The second set (JOP55_TR), taken on the 6th of September 1997, is almost identical to the first set, but consists of only two series of 14 frames each. The slit crossed the southern coronal hole and was slightly offset from the central meridian, to a position where the coronal hole extension was favourable at the time of the observations.

The third set consists of series of 12 different spectral frames each ($512 \times 360 \text{ pixels}$) taken during the SOHO roll manoeuvre on the 20th of March 1997. Series of frames were obtained every 30 degrees along the limb, with a larger number of exposures being made at the equator (total number of 190 frames, exposure time: 150 s). During the roll manoeuvre the slit was always oriented radially instead of being parallel to the N-S axis. This

data set includes about 50 identified and relatively unblended spectral lines.

Fig. 1 schematically represents the locations of the slit on the solar disk during the different sets of observations.

2.2. Data reduction

The following corrections have been made to the data before the analysis: A flat-field correction was applied using the flat-field image taken closest to the date of the respective observation. The geometrical distortion introduced by the detector has been reduced using the procedure supplied by the SUMER consortium. This routine compensates the pin cushion distortion of the image and, at the same time, corrects to a first approximation the inclination of the spectral lines with respect to the detector columns due to the alignment error between detector and grating. To obtain the correct locations on the Sun for the different spectral lines, their position along the slit on the detector has been measured as a function of wavelength and the displacement and magnification of the spectrometer have been compensated for. The data frames had been carefully selected beforehand to avoid intense lines, which would require corrections of saturation effects of the SUMER detectors, such as dead time or gain depletion.

2.3. Spectral line selection

The spectral ranges covered by the JOP55 and the roll observations do not exactly coincide. We selected 10 spectral regions (common to all data sets) containing interesting spectral lines for further analysis. Fig. 2 shows examples of three of the retained frames (spectra averaged in the spatial direction of each frame are plotted). They include coronal spectral lines, of Ne VIII and Fe XII, transition region lines, of N IV, O V and N V, as well as chromospheric lines, of O I, C I, Ni II and Si II.

A list of all the spectral lines retained for our analysis is given in Table 1. The formation temperatures of the corresponding ions have been taken from Arnaud & Rothenflug (1985). The formation temperature of lines of neutral species need to be treated with caution. More details can be found in Wilhelm & Inhester (2000, private communication).

Although other authors (Chae et al. 1998; Peter & Judge 1999) have pointed out problems with the S VI line at 933.39 \AA (anomalous center-to-limb variation), the results we obtained with this line are consistent with those obtained from other spectral lines. The parameter values derived for this line have therefore been retained when discussing the results.

2.4. Data analysis

The lines were identified using the line lists of Curdt et al. (1997) and Sandlin et al. (1986). For this analysis we selected lines that cover a wide range of formation temperatures. In addition, to facilitate data interpretation, lines with known strong blends have been avoided whenever possible. Line parameters are determined from fits of a Gaussian plus linear background to the

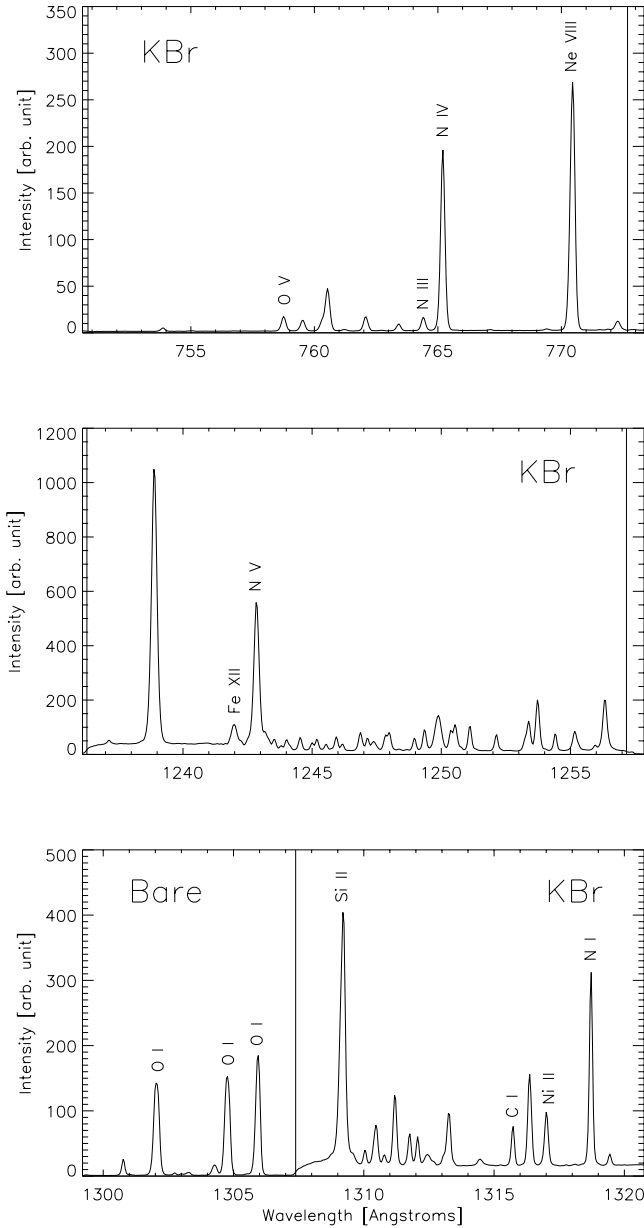


Fig. 2. Examples of analysed SUMER spectra. The upper two frames were recorded mainly on the potassium bromide (KBr) photocathode (within the two vertical lines) while the lowest frame shows a spectrum partially recorded on the bare microchannel plate and partially on KBr (separated by the vertical line). The spectra are averaged over the slit length. The analysed lines are identified.

spectrum at each spatial position. In cases in which a dominant line has one or more minor blends a routine fitting multiple Gaussians plus background has been employed to separate out the contributions of the blends. The number of Gaussian components used for the fit to each spectral line is listed in the last column of Table 1. Some lines, like C III 1175.71 Å have well separated components which allows us to apply multi-Gaussian fitting with success. Other lines such as Si II at 1309.28 Å have blends that are so well hidden and are so strongly variable relative to the line of interest that multi-Gaussian fits gave incon-

Table 1. Analysed spectral lines with the formation temperature † of the corresponding ion and the number of Gaussian components used for the fit.

Ion	Wavelength	Temperature	fitted Gaussians
O V	629.70	$2.35 \cdot 10^5$ K	2
S IV	661.44	$1.04 \cdot 10^5$ K	1
S IV	753.76	$1.04 \cdot 10^5$ K	1
O V	758.67	$2.35 \cdot 10^5$ K	1
N III	764.36	$8.04 \cdot 10^4$ K	1
N IV	765.15	$1.42 \cdot 10^5$ K	1
Ne VIII	770.43	$5.75 \cdot 10^5$ K	1
Ne VIII	780.32	$5.75 \cdot 10^5$ K	2
S VI	933.39	$1.74 \cdot 10^5$ K	1
C III	1175.71	$6.76 \cdot 10^4$ K	5
Si II *	1197.39	$1.27 \cdot 10^4$ K	1
Si III	1206.51	$3.00 \cdot 10^4$ K	1
Fe XII	1242.01	$1.41 \cdot 10^6$ K	4
N V	1242.80	$1.74 \cdot 10^5$ K	3
Si I	1258.80	$8.00 \cdot 10^3$ K	2
O I	1302.17	$1.51 \cdot 10^4$ K	1
O I	1304.86	$1.51 \cdot 10^4$ K	2
O I	1306.03	$1.51 \cdot 10^4$ K	1
Si II *	1309.28	$1.27 \cdot 10^4$ K	1
C I	1315.92	$1.44 \cdot 10^4$ K	1
Ni II	1317.22	$1.40 \cdot 10^4$ K	1
N I	1319.00	$1.62 \cdot 10^4$ K	1
C II	1334.50	$3.72 \cdot 10^4$ K	1
Si IV	1393.75	$7.08 \cdot 10^4$ K	1
O IV	1401.16	$1.66 \cdot 10^5$ K	2
Si IV	1402.80	$7.08 \cdot 10^4$ K	1

* Not used for the further analysis (see text)

† Warning: Formation temperatures listed are the temperatures of peak emissivity and may not reflect the actual formation temperature. Lines from optically dense regions require special consideration.

sistent results. For this reason, we do not consider both Si II lines in our sample for further analysis. A particularly difficult, but important case is that of the Fe XII line at 1242.01 Å. In coronal holes this line has blends that are almost as strong as the line itself. Consequently, it was quite difficult to fit, but a 4-Gaussian gave reasonable results, although with lower accuracy than the other lines. Due to its importance it has nevertheless been retained for the analysis.

The intensity, shift and width parameters of the selected lines were obtained at each spatial position from the best-fit Gaussians. This method turned out to be more precise for this kind of data than the moments method described by Doyle et al. (1997), which we used in a previous analysis (Stucki et al. 1999). For the analysis, we used the integrated intensity over the Gaussian fit to the spectral line profile.

The reference value for the shift has been chosen for each line separately as the mean value of the wavelength of the peak of the line profile averaged over the length of the slit. Thus the choice of reference for the shifts is not related to an absolute wavelength scale and has no influence whatsoever on the results. Since the shift values are unaffected by any instrumental

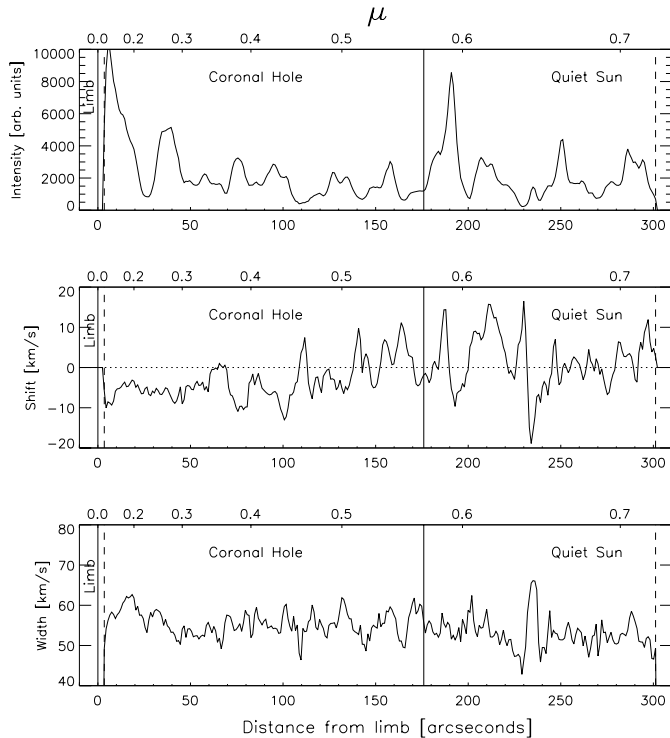


Fig. 3. An example of each of the fit parameters (intensity, shift and width) using the spectral profiles of N IV at 765.15 Å, obtained from the first set of observations (JOP055) as a function of distance from the limb. The coronal hole boundary is located approximately 176'' from the limb. It is marked by the vertical line near the center of the frame. The vertical solid line on the left, representing the position of the limb, is located just outside the limits of the image on the detector (dashed vertical lines) in this dataset. The scale at the top of each frame indicates $\mu = \cos \vartheta$, where ϑ is the heliocentric angle. Negative shifts signify blue shifts.

drift, we can derive relative shifts to a precision of about 1 kilometer per second depending upon the quality of the Gaussian fit. Although the slit often crossed the limb, only on-disk data are analysed.

The position along the slit of the boundary between the coronal hole and the quiet Sun has been deduced from whole-Sun images of the Fe XII 195 Å line of EIT (Extreme-ultraviolet Imaging Telescope, Delaboudinière et al. 1995) taken on the corresponding days.

An example of the variation of the line parameters along the slit is shown for the N IV (765.15 Å) line in Fig. 3. In the illustrated case we notice the presence of limb-brightening. Also, the line is on average blue-shifted inside the hole (relative to the average along the slit outside the hole) and somewhat broader. From this data set alone it is impossible to distinguish how much (1) the presence of the coronal hole, (2) the center-to-limb variation, and (3) intrinsic variability and spatial structure of the solar radiation contribute to the differences between the parameters in the hole and outside it.

In order to distinguish between these three sources we need, on the one hand, better statistics (i.e., more frames containing

the same spectral lines), and, on the other hand, also quiet-Sun data covering the same heliocentric angle as the coronal hole data (we define $\mu = \cos \vartheta$, where ϑ is the heliocentric angle). The roll data partly fulfill these requirements. By comparing the line parameters averaged over all profiles arising in the coronal hole with averaged line parameters from the quiet Sun at the same μ values it is in principle possible to distinguish between the center-to-limb variation and the hole-non-hole difference.

It is, however, still possible that we have not averaged over a sufficient number of data sets to reduce intrinsic solar variability to an acceptable degree. An idea of this residual intrinsic spatial variation of the line parameters is given by Figs. 4 and 5. They show the variations of line parameters along the slit for the N IV and Ne VIII lines, averaged over all quiet-Sun spectra as well as over all central meridian spectra of the roll data. The center-to-limb variation can be clearly seen in the intensity. Due to the relatively few spectra (three for the meridian and nine for the quiet Sun) the remaining variation of the intensity after the averaging is still large, in particular for N IV. By considering all available data (JOP055 and roll data) this variation can be further reduced. However, then the problem arises that the instrumental parameters underlying the data obtained along the meridian (containing the coronal hole) and those at other locations at the limb (quiet Sun; roll data) are not exactly the same. In order to counter this we also compare the line parameters obtained along the meridian, but outside the coronal hole, with those from the same μ values at other locations along the limb.

In total we had about 25 exposures of each spectral line at our disposal. In each exposure, we averaged the fit parameters in a sector corresponding to the position of the coronal hole (“small μ sector”), which means from $\mu = 0.1$ to $\mu \approx 0.5$, and in a sector corresponding to the quiet Sun (“large μ sector”), from $\mu \approx 0.5$ to $\mu \approx 0.67$. Those values were then averaged over all exposures taken at the meridian (containing northern or southern coronal hole regions), and over all exposures taken at other locations (roll data taken around the disk). Note that the actual coronal hole boundary in each exposure along the meridian (obtained from EIT Fe XII images) is used to distinguish between the small and large μ sectors, so that the μ values given above are only averages. We have tested whether inaccuracies in determining the coronal hole boundary may influence our results by introducing a “no-man’s-land” of about 40'' width between the small and large μ sectors. The line parameters of these pixels are not counted to either sector. We found that the results do not depend in any significant way on the presence or absence of such a “no-man’s-land”. The line parameters found are then related to the temperatures of maximum abundance of the ions taken from Arnaud & Rothenflug (1985).

3. Results

3.1. Comparison of line parameters

Fig. 6 shows the relative difference of the averaged intensity at the meridian to that at the other positions along the limb. It was calculated using the expression $2 \cdot (I_{\text{meridian}} - I_{\text{other locations}}) / (I_{\text{meridian}} + I_{\text{other locations}})$. As described in Sect. 2.4, the data at

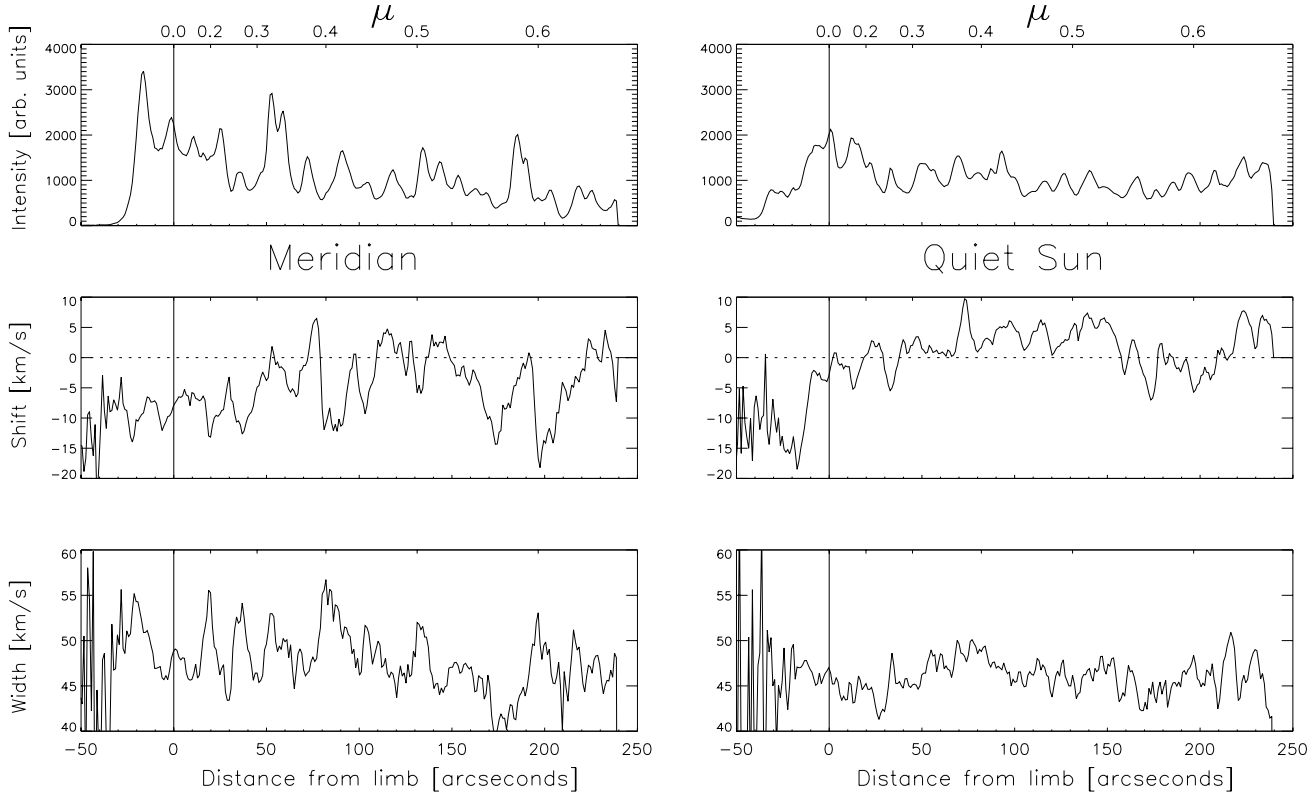


Fig. 4. Line parameters (intensity, shift and width) of the spectral profiles of N IV at 765.15 Å obtained in the third set of observations (roll data), averaged over all available data (nine images) in the quiet Sun (right frame) and averaged over all central meridian data (left frame, three images).

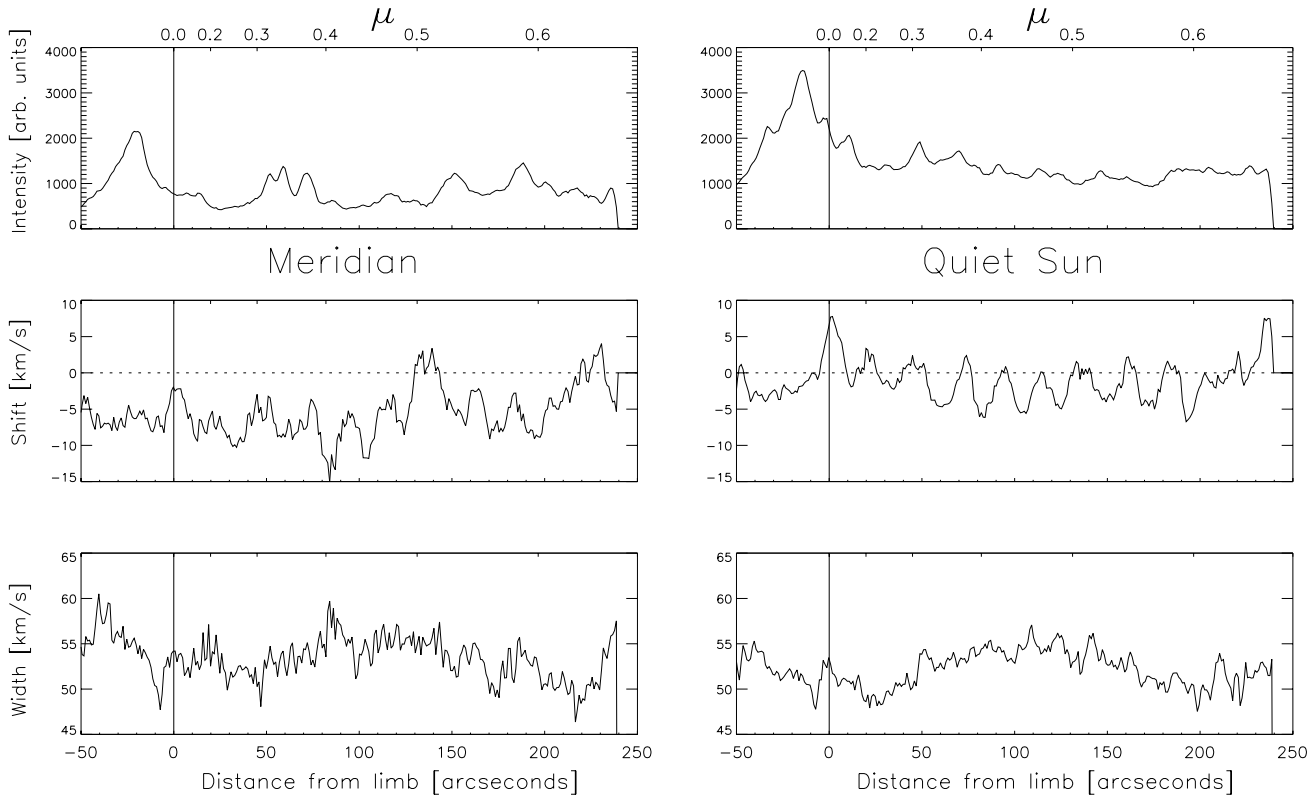


Fig. 5. Same as Fig. 4 for Ne VIII at 770.43 Å

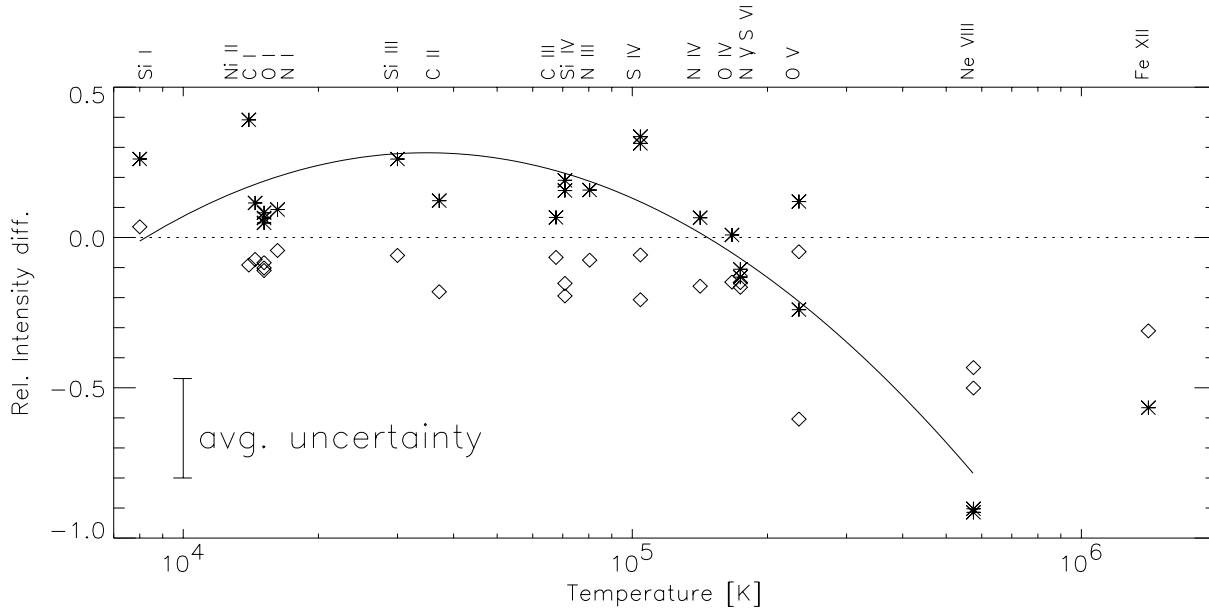


Fig. 6. Relative intensity difference between the meridian and the other locations along the limb vs. formation temperature. Diamonds: large μ sector (only quiet Sun); Stars: small μ sector (including coronal hole). The solid line shows a second order polynomial fit to the stars. Due to the larger uncertainty of the parameters of the Fe XII line, its value is not used for the regression. A representative error bar is also plotted (see text for details).

small μ and at large μ were treated individually and are represented by different μ symbols in Fig. 6. The stars represent the relative difference for the data in the spatial range near the limb (small μ sector). The diamonds represent this difference for the data in the spatial range closer to disk center (large μ sector). The stars are thus representative of the difference between coronal hole and quiet-Sun regions. For the hottest lines, the relative intensity is smaller for data sampled in a coronal hole than for the quiet Sun, in agreement with expectations. The large μ sector, which is outside the hole for every location, also shows a smaller emission for the meridian data. The effect is nevertheless smaller than for the actual coronal hole. The reason for this behaviour is unknown. A possible explanation is the fact that we observed the Sun at activity minimum, when it has well defined streamer belts at low latitudes. Thus line-of-sight effects could lead to excess brightness in low latitude coronal lines compared to the quiet-Sun at high latitudes. It does suggest, however, that to some extent the plasma at the meridian, but outside the coronal hole boundary (as deduced from EIT images), exhibits the main property of a coronal hole, namely less intense emission from hot ions. We cannot rule out, however, that the behaviour of the large μ data points is dictated simply by the intrinsic solar variation. For example, the scatter shown by the large μ data points suggests that there is still some residual solar variation, even after averaging over all the available data.

In Fig. 6 (as well as in Figs. 7 and 8) the average uncertainty has been calculated using the standard deviation for each parameter of the Gaussian fit obtained at each spatial pixel, and averaged over all the data available for a given spectral line. The plotted uncertainty is thus a measure of the scatter of the parameter values of a given spectral line. The statistical uncertainty

of the plotted (averaged) parameters are considerably smaller than the plotted one. The uncertainty obtained for three typical spectral lines have been averaged to get a representative value.

Fig. 7 shows the difference between the line widths observed on the meridian (data with coronal hole at small μ and quiet Sun at large μ) and those observed at other locations (only quiet Sun) at the same μ ($W_{\text{meridian}} - W_{\text{other locations}}$).

Almost all spectral lines are broader inside the coronal hole, which confirms similar results found by Lemaire et al. (1999). This increase in line width indicates higher non-thermal velocities inside coronal holes. The Fe XII line exhibits an anomalous behaviour in the sense that it does not follow the trend exhibited by the other lines. Blends from cooler ions in its wings may contribute to this. The widths of the lines in the large μ sector at the meridian again display the same behaviour as the small μ data, although less clearly. This strengthens the case for the interpretation, made on the basis of the diamonds in Fig. 6, that the large μ sector at the meridian behaves like a weak coronal hole.

If we assume that the Doppler width resulting from temperature is the same at the meridian as at the other locations then we can calculate the difference in turbulent velocity. This difference is given by

$$\Delta\xi_T = \sqrt{\xi_{T,\text{meridian}}^2 - \xi_{T,\text{other locations}}^2}.$$

For our data (averaged over all spatial pixels and spectral lines) we obtain:

$$\Delta\xi_T = 13.2 \text{ km s}^{-1} \text{ for small } \mu \text{ (coronal hole)}$$

$$\Delta\xi_T = 9.1 \text{ km s}^{-1} \text{ for the large } \mu \text{ sector}$$

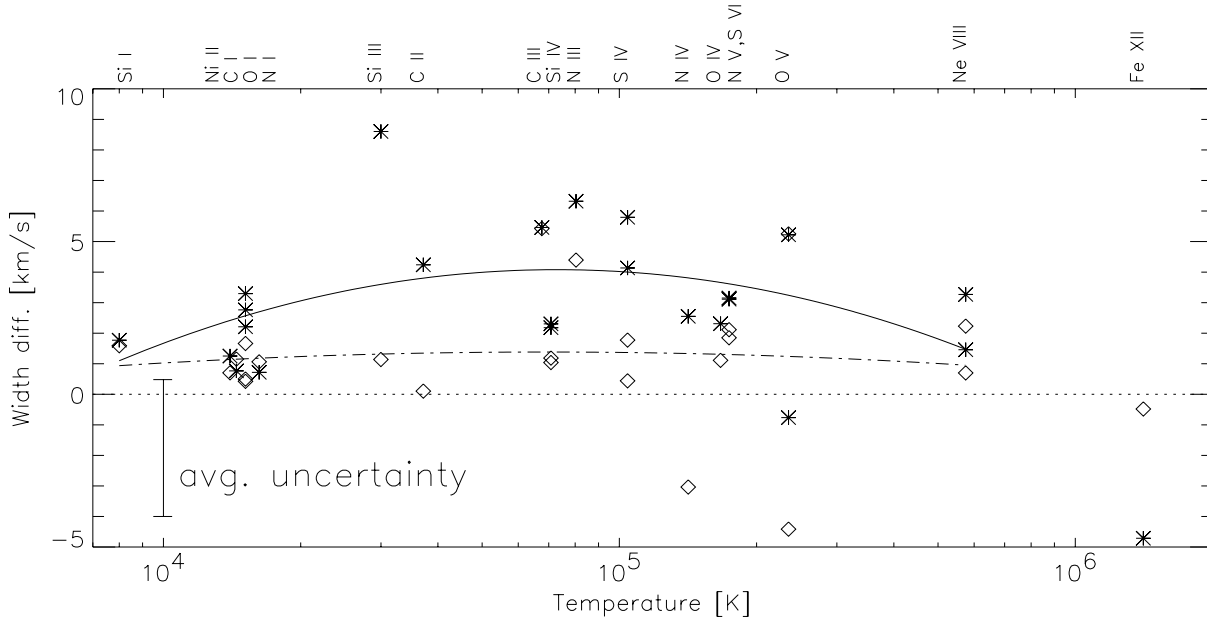


Fig. 7. Width difference vs. formation temperature. The “width difference” represents the difference between the line width observed on the meridian and that at other locations. Diamonds: large μ sector; Stars: small μ sector (i.e. widths of hole profiles relative to non-hole profiles). The solid line shows a second order polynomial fit to the small μ sector points, while the dot-dashed line shows a fit to the large μ sector points.

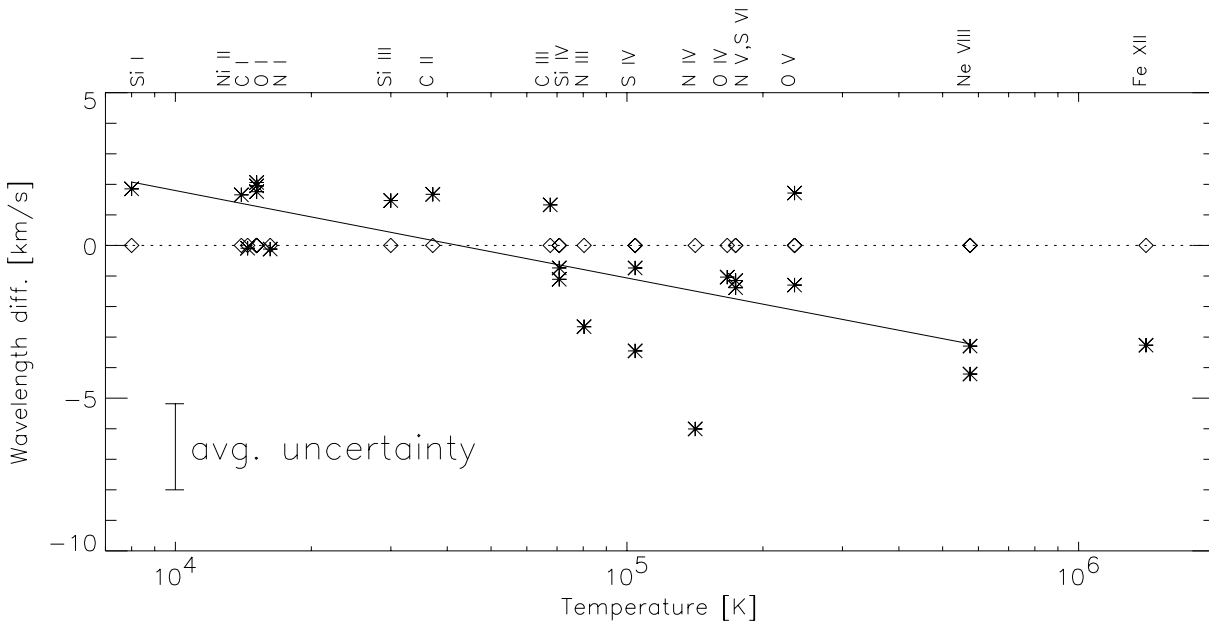


Fig. 8. Wavelength difference in velocity units vs. formation temperature. The “wavelength difference” represents the difference between the wavelength observed on the meridian and the one observed at other locations at the same μ . Since the wavelength scale is not absolute, we equalized the wavelengths at the meridian and the equator outside the hole. Diamonds: large μ sector (identically zero due to equalization); Stars: small μ sector (i.e., shift of hole profile relative to non-hole profiles). The solid curve shows a second order polynomial fit to the small μ sector points. Negative shifts signify blueshifts.

Fig. 8 displays the difference between the wavelengths observed on the meridian (data with coronal hole) and the ones observed at other locations (purely quiet Sun) at the same μ . Since the wavelength scale does not have an absolute calibration, we equalized the shifts between meridian data and other data for the sector outside the hole (large μ) by adding

$\Delta\lambda = \lambda_{\text{other}} - \lambda_{\text{meridian}}$ to the $\lambda_{\text{meridian}}$, where $\lambda_{\text{meridian}}$ and λ_{other} are averaged over all data sets at large μ . The same offset, $\Delta\lambda$, was then also added to the shifts of the meridian data in the small μ sector. In this manner the line shifts in the coronal hole can be determined relative to the shifts in the quiet Sun at equal μ , i.e., close to the limb. Fig. 8 shows a distinct blueshift rela-

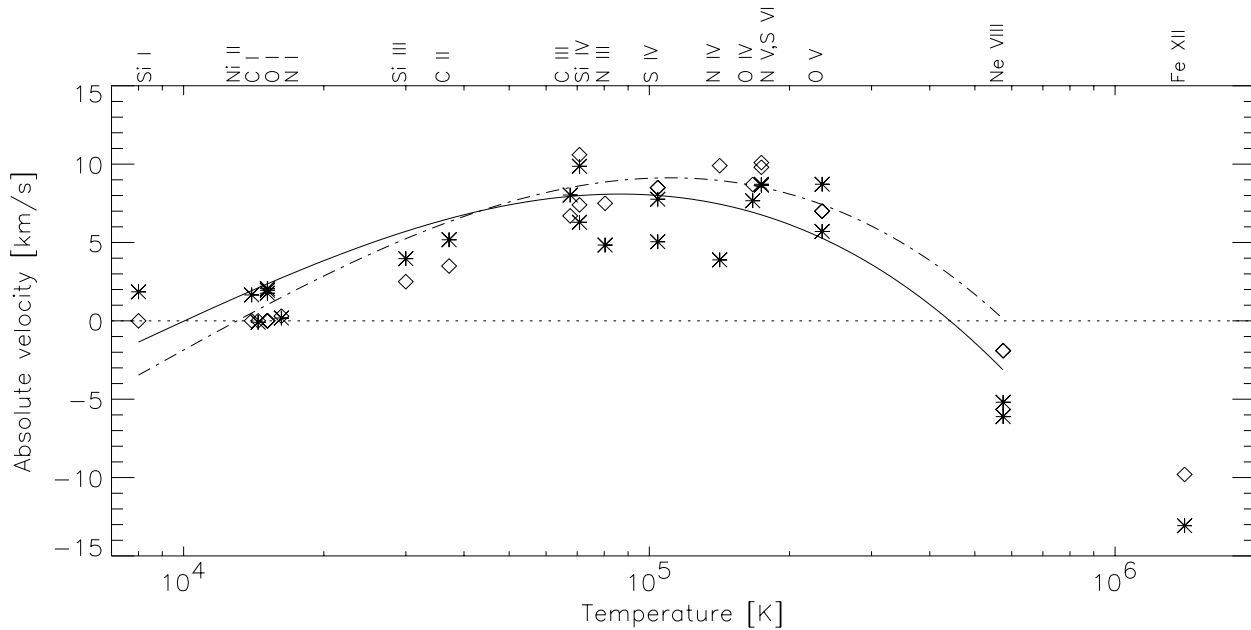


Fig. 9. Absolute wavelength shift in velocity units vs. formation temperature. The absolute shifts are determined using the data of Teriaca et al. (1999). Diamonds: large μ sector; Stars: small μ sector. The solid curve shows a third order polynomial fit to the small μ sector points while the dot-dashed curve shows a similar fit to the large μ sector points. Negative shifts signify blueshifts.

tive to the quiet Sun at high temperatures in the coronal hole and a small redshift at low temperatures. Hence there is a steadily increasing relative blueshift with temperature. This may represent evidence of solar wind outflow at low altitudes in coronal holes, as has been previously concluded by Hassler et al. (1999) and Wilhelm et al. (2000). The small μ sector points in Fig. 8 may actually underestimate the trend, if the large μ sector at the meridian also weakly exhibits coronal hole properties, as suggested by Figs. 6 and 7. In that case, lines formed there are also expected to be shifted relative to the quiet Sun.

To express our results in terms of absolute speeds, we can use line shifts found by other authors in the quiet Sun (Doschek et al. 1976; Brekke et al. 1997; Teriaca et al. 1999). Fig. 9 shows the results for coronal-hole and quiet-Sun regions with respect to the shift values obtained by Teriaca et al. (1999). As expected, the curve laid through the quiet-Sun symbols follows exactly Teriaca's curve.

The Ne VIII 770.43 Å line has also been analysed in detail by Dammasch et al. (1999). He found line shifts of -6.2 km s^{-1} in coronal holes and -0.8 km s^{-1} for the quiet Sun. This is in very good agreement with our values (-6.1 and -1.9 km s^{-1}).

Fig. 9 reveals how small the differences between quiet-Sun and coronal-hole regions are with respect to the temperature dependence of the wavelength shift. In particular, only the coronal lines show a true blueshift (both inside and outside the coronal hole), which is not significantly larger than the redshift exhibited by the transition region lines (even in the coronal hole). In view of this result one may need to be more cautious about assigning the small extra blueshift within coronal holes to the initial phase of the fast solar wind, since it may have to do with (small) changes in the mechanism giving rise to the red- and

blueshifts observed in the quiet Sun. It would be useful to have observations of additional coronal lines to put this conclusion on a more sound basis.

3.2. Distribution of intensities

Next we try to characterize better the intensity differences between coronal hole and quiet-Sun regions in view of the unexpected brightening displayed by chromospheric and some transition region lines in coronal holes (Fig. 6). To this end, we plot the intensity histograms for four representative lines belonging to N I, Ni II, O IV and Ne VIII in Figs. 10 to 13. Here we have put the intensities from all spatial pixels into 35 bins. We plotted the histogram for the small μ sector at the meridian (i.e., the coronal hole data), for the small μ sector at other locations and finally for the large μ sector at other locations (the large μ sector data at the meridian have not been included to avoid cluttering the figures). The chromospheric lines (N I and Ni II) show a higher average intensity inside the coronal hole area (Figs. 10 and 11). It appears that in the coronal hole more bright network locations exist than in the quiet Sun. The Ni II line exhibits a higher contrast, i.e., a wider distribution in the coronal hole. In the case of N I, however, the whole distribution appears to be shifted to higher intensities. These histograms show that the higher intensities shown by these lines in the coronal hole are of solar origin and are not due to some calibration problem (which would have led to the histograms in coronal hole and quiet Sun being the same within a multiplicative factor). To what extent the larger network contribution in the coronal hole is due simply to insufficient statistics (too few sampled points) is as yet unknown. Alternatively, it may be a result of the fact that the magnetic

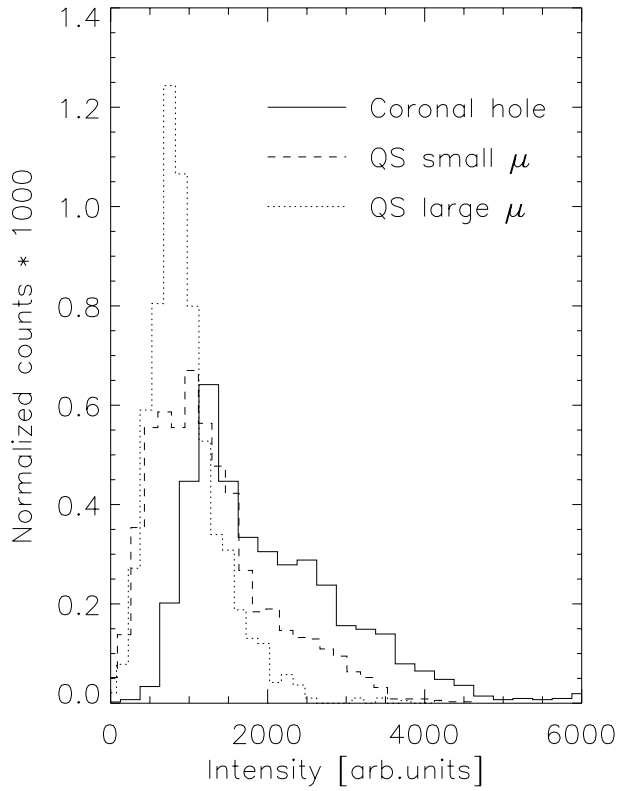


Fig. 10. Intensity histogram of the N I line at 1319.0 Å. Solid line: meridian data in the small μ sector, i.e., in the coronal hole. Dashed line: quiet Sun data in small μ sector. Dotted line: quiet Sun data in large μ sector, at locations away from the meridian.

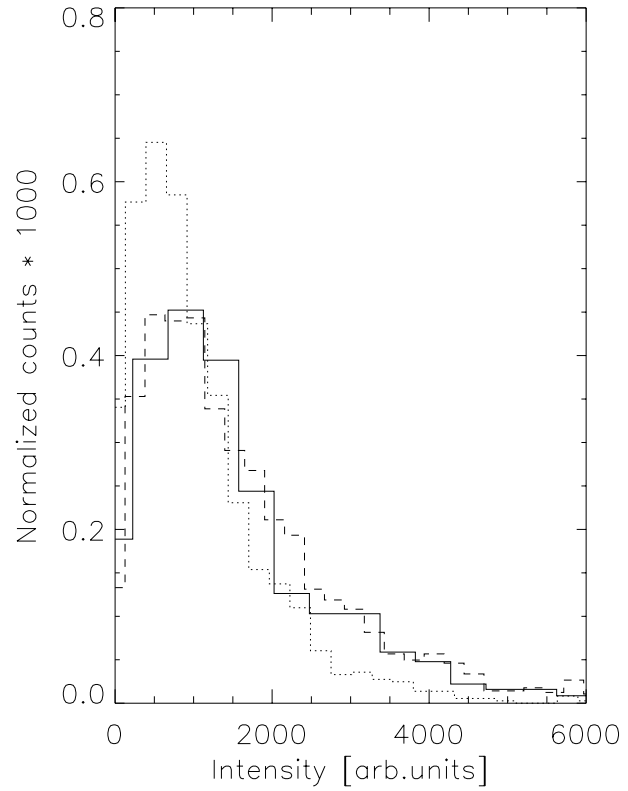


Fig. 12. Same as Fig. 10 for O IV at 1401.16 Å.

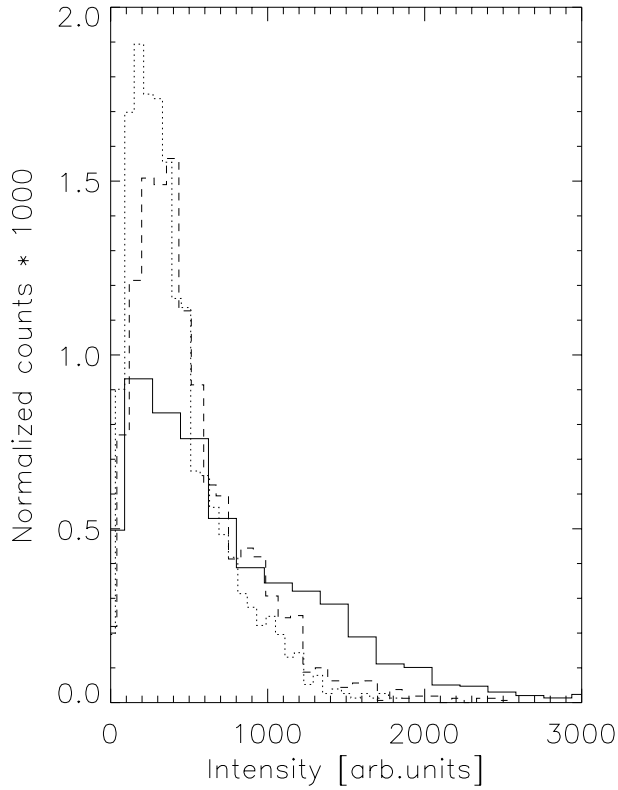


Fig. 11. Same as Fig. 10 for Ni II at 1317.22 Å.

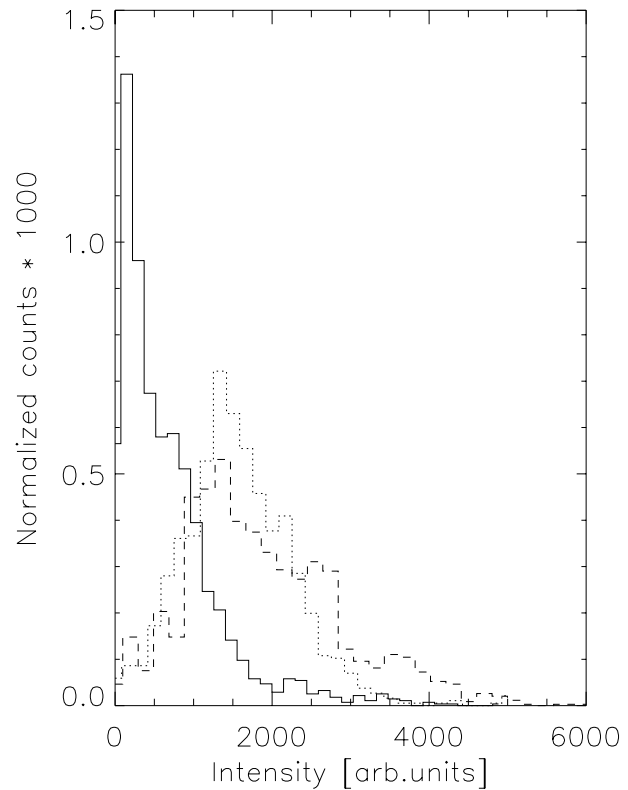


Fig. 13. Same as Fig. 10 for Ne VIII at 770.43 Å.

filling factor (i.e. fractional area covered by magnetic field) in regions with significant excess of one polarity typically underlying coronal holes is a factor of approximately two larger than in the normal (mixed polarity) quiet Sun (Zhang et al. 1997). Since chromospheric and transition-region spectral lines are as a rule brighter in regions with higher magnetic filling factor, this might explain the somewhat larger brightness of such spectral lines in the coronal hole.

The typical transition-region line O IV at 1401.16 Å exhibits no significant difference in the intensity distribution of the network (Fig. 12). Finally, in the coronal line (Ne VIII at 770.43 Å) the distribution in the coronal hole is much narrower than in the quiet Sun (Fig. 13). This is in agreement with the results obtained by Gallagher et al. (1998) with data from the Coronal Diagnostic Spectrometer (CDS) onboard SOHO (Harrison et al. 1995). In all cases the difference between the dashed and dotted curves indicates the center-to-limb variation in the quiet Sun.

4. Conclusions

We have analysed the line intensity, shift, and width of 26 spectral lines observed by SUMER in polar coronal holes and compared these with the corresponding parameters determined in quiet-Sun regions.

We find evidence for the presence of a coronal hole through strongly reduced intensity in spectral lines formed above $5 \cdot 10^5$ K. The distribution of intensities shows more bright network inside coronal holes for chromospheric lines, but this effect disappears in transition-region lines. The paucity of the statistics means that it is important to study such distributions with considerably larger data sets, as has recently been done by Pauluhn et al. (2000) for the quiet Sun. The line widths are found to be larger inside coronal holes. The excess widths correspond approximately to excess turbulence velocities of $10 - 15 \text{ km s}^{-1}$ in coronal holes.

A blueshift in the coronal hole relative to the quiet Sun is shown by all the lines with formation temperatures above 10^5 K, and it increases with temperature. The interesting possibility that the blueshifts observed by Hassler et al. (1999), Wilhelm et al. (1998b, 2000) and Dammasch et al. (1999) reveal the solar wind acceleration in the polar coronal holes needs further examination. We have extended the work of these authors in that we consider a larger number of spectral lines. We have also focussed on the wavelength shifts in quiet sun and coronal holes separately (determined under the assumption that the quiet-Sun shifts derived by Teriaca et al. are correct). These reveal that the shifts between lines in coronal holes and the quiet Sun are small compared to the shifts exhibited by the lines in the quiet Sun. This indicates some caution in attributing the *relative* blueshifts observed in coronal holes to the fast solar wind.

It would be of great interest to have better access to the properties of the coronal gas in a hole, in order to try to follow plasma movements in hotter gas. The scarcity of truly coronal lines in the SUMER spectral range, and in particular in the analysed data, is a hinderance. The CDS instrument onboard SOHO may give further insight by providing the possibility of analysing more lines with higher formation temperatures as well as with better statistics, although with lower spatial and spectral resolution. Such work is currently in progress.

Acknowledgements. SOHO is a mission of international cooperation between ESA and NASA. The SUMER project is financially supported by DLR, CNES, NASA, and the ESA PRODEX programme (Swiss contribution). This work was partly supported by the Swiss National Science Foundation, grant No. 20-55456.98, and by a grant from the ETH-Zürich which are gratefully acknowledged.

References

- Arnaud M., Rothenflug R., 1985, *A&AS* 60, 425
 Brekke P., Hassler D.M., Wilhelm K., 1997, *Solar Phys.* 175, 349
 Chae J., Yun H.S., Poland A.I., 1998, *ApJS* 114, 151
 Curdt W., Feldman U., Laming J.M., et al., 1997, *A&AS* 126, 281
 Dammasch I.E., Wilhelm K., Curdt W., et al., 1999, *A&A* 346, 285
 Delaboudinière J.-P., et al., 1995, *Solar Phys.* 162, 291
 Doschek G.A., Feldman U., Bohlin J.D., 1976, *ApJ* 205, L177
 Doyle J.G., O'Shea E., Erdélyi R., et al., 1997, *Solar Phys.* 173, 243
 Gallagher P.T., Phillips K.J.H., Harra-Murnion L.K., et al., 1998, *A&A* 335, 733
 Harrison R.A., Sawyer E.C., Carter M.K., et al., 1995, *Solar Phys.* 162, 233
 Hassler D.M., Dammasch I.E., Lemaire P., et al., 1999, *Sci* 283, 810
 Hollweg J.V., 1991, In: Ulmschneider P., Priest E.R., Rosner R. (eds.) *Mechanisms of Chromospheric and Coronal Heating*. Springer Verlag, p. 423
 Huber M.C.E., Foukal P.V., Noyes R.W., et al., 1974, *ApJ* 194, L115
 Lemaire P., Bocchialini K., Aletti V., et al., 1999, *Space Sci. Rev.* 87, 249
 Marsch E., 1997, In: Vial J.-C., Bocchialini K., Boumier P. (eds.) *Space Solar Physics*. Springer Verlag, p. 107
 Pauluhn A., Solanki S.K., Rüedi I., et al., 2000, *A&A* 362, 737
 Peter H., 1999, *ApJ* 516, 490
 Peter H., Judge P.G., 1999, *ApJ* 522, 1148
 Sandlin G.D., Bartoe J.-D.F., Brueckner G.E., et al., 1986, *ApJS* 61, 801
 Stucki K., Solanki S.K., Rüedi I., et al., 1999, *Ap&SS* 264
 Teriaca L., Banerjee D., Doyle J.G., 1999, *A&A* 349, 636
 Tu C.-Y., Marsch E., Wilhelm K., et al., 1998, *ApJ* 503, 475
 Wilhelm K., Curdt W., Marsch E., et al., 1995, *Solar Phys.* 162, 189
 Wilhelm K., Lemaire P., Dammasch I.E., et al., 1998a, *A&A* 334, 685
 Wilhelm K., Marsch E., Dwivedi B.N., et al., 1998b, *ApJ* 500, 1023
 Wilhelm K., Dammasch I.E., Marsch E., et al., 2000, *A&A* 353, 749
 Zhang L.D., Zirin H., Marquette W.H., 1997, *Solar Phys.* 175, 59